Dalton Transactions



PAPER View Article Online
View Journal | View Issue



Cite this: *Dalton Trans.*, 2025, **54**, 3071

Received 19th November 2024, Accepted 7th January 2025 DOI: 10.1039/d4dt03231d

rsc.li/dalton

A rare case of a zero-field single-ion magnet in a cerium(III) pseudo-icosahedral complex†

Jarrod R. Thomas, ¹D^a Marcus J. Giansiracusa, ¹D* Jonathan T. Mifsud, ^a Richard A. Mole ¹D^c and Scott A. Sulway ¹D* *^a

The synthesis and structural characterisation of $[Ln(Tp^{2-Fu})_2]I$ (1-Ln; Ln = La, Ce, Pr, Nd) $(Tp^{2-Fu}) = hydrotris (3-(2'-furyl)-pyrazol-1-yl)borate)$ have been reported as an isomorphous series adopting pseudo-icosahedral ligand field geometries. Continuous shape measurement (CShM) analyses on the crystal field environments of 1-Ln show the smallest values yet reported for complexes employing two hexadentate ligands (e.g. bis-scorpionate environments), with the smallest belonging to 1-La. Single-ion magnetism for 1-Ce, 1-Pr and 1-Nd was probed with ac magnetic susceptibility studies revealing slow magnetic relaxation for 1-Nd in applied magnetic fields and in zero-applied field for 1-Ce, which is a rare observation for Ce(III)-based single-ion magnets. The energy barrier to magnetic relaxation for 1-Ce was experimentally determined to be $U_{eff} = 30(5) \text{ cm}^{-1}$, which is comparable to that of other cerium-based single-molecule magnets in the literature, where these systems stablise the $m_J = \pm 5/2$ state and possess large energy gaps between the ground and first excited state that do not agree with the experimentally determined barrier.

Introduction

Early lanthanide single-ion magnets (SIMs) are generally underrepresented due to the ions possessing relatively small spin angular momentum, S, and correspondingly coupled spinorbit angular momentum, J, when compared to the recent success within the field using mid-to-late lanthanides. ^{1–11} Along with the small magnetic moments of early lanthanides, low coordination numbers are not favoured due to the intrinsic size of the lanthanide(III) ions, which has been a major discussion point for the success of lanthanocerium-based SIMs. However, the spin multiplicity and coordination number of lanthanide-based SIMs are not the only dependency of high performing SIMs; ligand field geometries and the (non-) Kramers nature of the lanthanide ion both play an integral role in the overall slow magnetic relaxation behaviour. ¹²

A recently charted ligand field for lanthanide-based SIMs is that of icosahedral geometry, which has been expanded by us through the use of hexadentate scorpionate ligands in complexes such as [Ln(Tp^{2-py})₂](BPh₄) (2-Ln; Ln = La, Ce, Pr, Nd,

Sm, Eu, Gd, Tb, Dy; $Tp^{2-py} = hydrotris(3-(2'-pyridyl)-pyrazol-1-yl)borate)$ and $[Ln(Tp^{2-Fu})_2](BPh_4)$ (3-Ln; Ln = Ce, Dy; Tp^{2-Fu} =

Synthesis and solid-state characterisation

Synthesis of pseudo-icosahedral *bis*-scorpionate lanthanide complexes is generally a straightforward metathetical reaction, being first demonstrated by McCleverty and Ward in the 1990's with the isolation of [Ln(Tp^{2-py})₂](BPh₄) (2-Ln; Ln = La, Sm, Eu, Gd, Tb). ^{15,16} We have since extended the homologous series for 2-Ln to cerium, praseodymium, neodymium and dysprosium. However, the latter requires an inert synthesis due to large coordination numbers not being favoured for the late

hydrotris(3-(2'-furyl)-pyrazol-1-yl)borate). hydrotris(3-(2'-furyl)-pyrazol-1-yl)borate). The early lanthanide containing complex [Ce(Tp $^{2-py}$)₂](BPh₄) **2-Ce** exhibited field-induced slow magnetic relaxation; however, due to the complexity of the ligand field environment and pseudo-spherical nature of the charge distribution about the cerium(III) centre, the dominating magnetic relaxation occurs *via* a Raman mechanism. Thus by the fine tuning of the scorpionate ligand used, we present the synthesis and characterisation of [Ln(Tp $^{2-Fu}$)₂]I (**1-Ln**; Ln = La, Ce, Pr, Nd) by single crystal X-ray diffraction and magnetometry with supporting *ab initio* calculations. Herein, we explore the effects of heteronuclear hexadentate ligands on the slow magnetic relaxation in highly symmetric lanthanide-based SIMs.

Results and discussion

^aSchool of Chemistry, The University of New South Wales (UNSW), Kensington, Sydney, 2052, Australia. E-mail: s.sulway@unsw.edu.au

^bSchool of Chemistry, University of Melbourne, Parkville, Victoria, 3010, Australia. E-mail: marcus.giansiracusa@unimelb.edu.au

^cThe Australian Nuclear Science and Technology Organisation, Lucas Heights, NSW 2323, Australia

[†]Electronic supplementary information (ESI) available. CCDC 2395485-2395488. For ESI and crystallographic data in CIF or other electronic format see DOI: https://doi.org/10.1039/d4dt03231d

(Fig. S1†).

Paper

lanthanides. 13 Furthermore, we have exemplified the use of the furyl substituted ligand Tp^{2-Fu} in [Ln(Tp^{2-Fu})₂](BPh₄) (3-Ln) for Ln = Ce and Dy, where again the latter undergoes a 1,2-borotropic shift to favour a lower coordination number. 14 The synthetic routes to 3-Ln used sodium salts due to the availability and solubility of NaBPh4, although NaTp2-Fu did not have similar solubility, and the yields of these reactions are low. Thus, to optimise these reactions the use of the potassium salt KTp^{2-Fu} and the counter-ion of iodide, inspired by the uranium(III) complex [U(Tp^{2-py})₂]I, ¹⁶ allowed the isolation of 1-Ln in large yields (64-89%) from a one-pot reaction in methanol (Scheme 1) and later extracted with CH2Cl2. Single crystals suitable for X-ray diffraction of 1-Ln-(CH₂Cl₂)₂ were obtained via Et₂O vapour diffusions of 1-Ln dissolved in CH₂Cl₂. The ATR-FTIR spectra of 1-Ln·(CH₂Cl₂)₂ are superimposable (Fig. S2 and S3†), suggesting the same structural composition. Due to the paramagnetic nature of 1-Ce, 1-Pr and 1-Nd the NMR spectra were not collected; however, the ¹H and ¹¹B spectra for 1-La were collected in d_6 -DMSO and present near

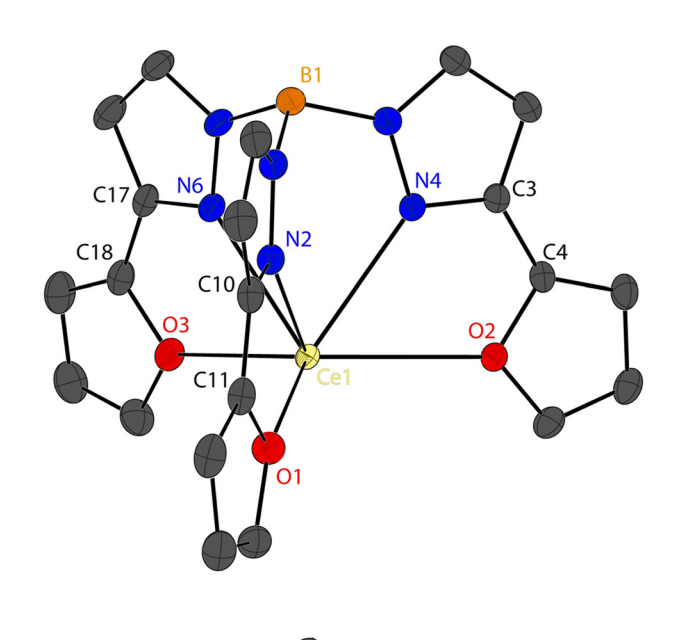
The same synthetic procedure was attempted using hydrated EuCl₃ and SmCl₃ as lanthanide sources but recrystallisation resulted in discolouration and powdered samples. As per our previous publications, the size of the lanthanide ion plays a crucial role in the stability of twelve coordinate *bis*-scorpionate lanthanide complexes.^{13,14} The proximity of the scorpionate ligand, and the deviation from perfect ligand fields (measured by continuous shape measurements (CShM), *vide infra*), can be used to predict when these twelve-coordinate systems become unstable. We have attributed 1,2-borotropic shifting of the Tp^{2-Fu} ligand as the likely cause for us not being able to isolate **1-Eu** and **1-Sm** given the relatively small lanthanide ions in these systems.¹⁴

identical spectra to the alkali salts of the Tp^{2-Fu} ligand

The isomorphous 1-Ln· $(CH_2Cl_2)_2$ series pack in the triclinic space group $P\bar{1}$ (the solid-state structure for the ion-pair for 1-Ce is shown in Fig. 1 and the remaining compounds in Fig. S4–S6;† coordination geometries from the cations in 1-Ln and B···B axis views are shown in Fig. 2 and selected atomic distances and angles have been summarised in Table 1). When comparing the unit cell dimensions of 1-Ln· $(CH_2Cl_2)_2$, there are no obvious trends, though the volume of each cell decreases, attributed to the lanthanide contraction (Fig. S8†). The cations in 1-Ln have inversion symmetry where one scorpionate ligand comprises the asymmetric unit, akin to that of 2-Ln, 13 with a lanthanide ion and counter-ion of iodine having half occupancies (Fig. 1). The unit cell consists of one ion pair with two CH_2Cl_2 molecules (Fig. S7†). The iodide ions occupy

$$LnCl_3$$
: $xH_2O + 2 KTp^{2-Fu} + KI \xrightarrow{MeOH} [Ln(Tp^{2-Fu})_2]I$
 $Ln = La, Ce, Pr, Nd$

Scheme 1 Synthetic route to **1-Ln** (Ln = La, x = 7; Ln = Ce, x = 6; Ln = Pr, x = 6, Ln = Nd, x = 6).



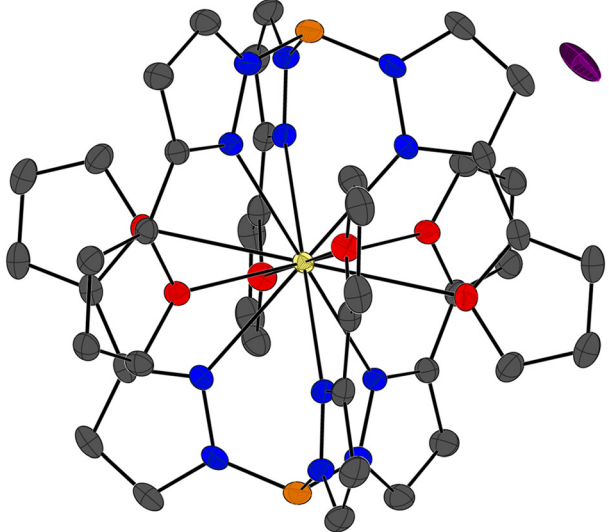


Fig. 1 Solid-state structures of the cation in the asymmetric unit (top) and the ion pair (bottom) in $1-Ce\cdot(CH_2Cl_2)_2$, drawn with a 50% ellipsoid. Cerium(III) = cream, iodine = purple, oxygen = red, nitrogen = blue, carbon = grey, boron = orange; hydrogen atoms and lattice solvents have been omitted for clarity.

the corners of the unit cell and lie on inversion points, and analogously the lanthanide ions also lie on inversion points yet are located at the centre of the cells. Due to the lanthanide lying on an inversion point the second Tp^{2-Fu} is generated by symmetry which results in all X–Ln–X (X = coordinating atoms) angles being 180° alongside the B···Ln···B angle being linear and the molecule possessing a pseudo- S_6 axis down the B···B axis (Fig. 2).

The ligand field geometries present in **1-Ln** are pseudo-ico-sahedral (Fig. 2) with the CShM values being below 0.4 for all compounds. The smallest CShM is observed in **1-La** (CShM(I_c) = 0.340) and gradually increases across the lanthanide series. To our knowledge these are the smallest CShM values of I_c geo-

Dalton Transactions Paper

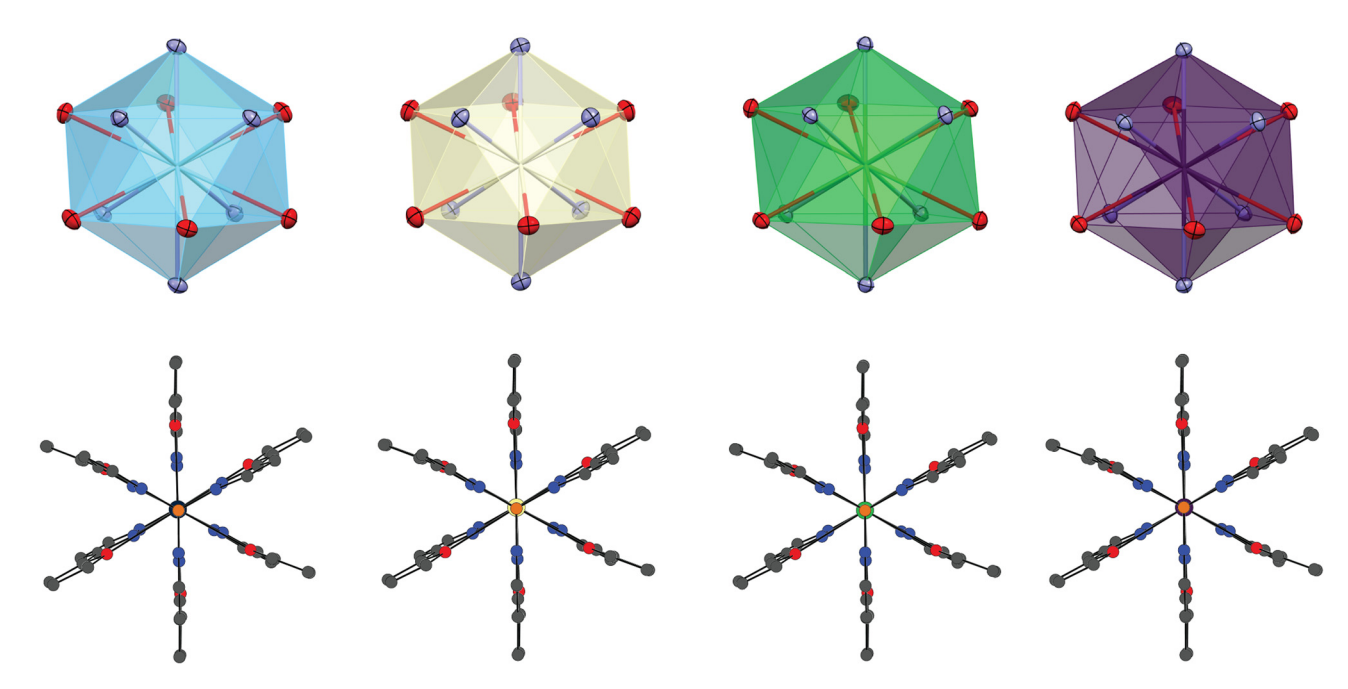


Fig. 2 Coordination geometries of the metal centres in 1-Ln (top), shown with coordinated atoms drawn with 50% ellipsoids and view from the B...B axis (bottom). Metal centres are lanthanum, cerium, praseodymium and neodymium going from left to right. The colour scheme is defined in Fig. 1.

Table 1 Selected bond/atomic distances and angles for 1-Ln

	1-La	1-Ce	1-Pr	1-Nd
Ln···B/Å	3.891(7)	3.872(5)	3.861(5)	3.846(5)
$Ln-N_{pz}/\mathring{A}$	2.670(2)-2.683(2)	2.6502(15)-2.6641(15)	2.6354(14)-2.6528(14)	2.624(2)-2.643(2)
Ln–O _{Fu} /Å	2.8819(19)-2.8688(18)	2.8478(13)-2.8753(13)	2.8424(12)-2.8680(12)	2.8390(17)-2.8674(17)
Conical angle ^a /o	43.06-43.23	42.85-43.16	42.70-43.07	42.70-43.12
Furyl torsion ^b /o	1.2(4)-8.5(5)	0.4(3)-9.1(3)	0.4(2)-9.4(3)	0.6(3)-8.9(3)
Ln…Ln/Å	11.1211(8)	11.0781(6)	11.0573(5)	11.0672(6)
$CShM(I_c)$	0.340	0.352	0.362	0.391

^a Conical angles are taken from N2-B1-Ln1, N4-B1-Ln1 and N6-B1-Ln1 (Ln = La, Ce, Pr, Nd). ^b Magnitude of the torsion angles is measured between N2-C3-C4-O4, N4-C10-C11-O2 and N6-C17-C18-O3.

metry for two hexadentate ligands; in particular, these are the smallest for bis-scorpionate complexes, or tripodal ligands in general. The smaller CShM values are attributed to the different 'bite' angle of the Tp2-Fu ligand (conical angle, Table 1). The five membered furyl rings produce differing coordination bond distances, conical angles (Ln1-B1-N2, Ln1-B1-N4 and Ln1-B1-N6) and furyl torsion angles (N2-C3-C4-O1, N4-C10-C11-O2 and N2-C17-C18-O3) when compared to the analogous $\mathrm{Tp}^{2\text{-py}}$ ligand, where the smallest $\mathrm{CShM}(I_{\mathrm{c}})$ is 0.362, seen in 2-Ce. 13 The coordinating distances of both the nitrogen atoms from the pyrazolyl group (N_{pz}) and the oxygen atoms from the furyl groups (O_{Fu}) gradually decrease across the lanthanide series, which is seen in the 2-Ln series and is an excellent physical observation of lanthanide contraction.¹³ The coordination distances in 1-Ln are shorter than that of 2-Ln, which again is due to the different bite of the ligands allowing the scorpionate ligand to reside closer to the lantha-

nide ions, evident by the shorter B...Ln distances (3.891(7)-3.846(5) Å cf. 3.923(7)-3.904(6) Å when comparing **1-Ln** to **2-Ln** respectively, for Ln = La, Ce, Pr, Nd). 13 The solid-state packing of 1-Ln·(CH₂Cl₂)₂ allows for well-spaced lanthanide ions, which are defined by the a-axis with the smallest intermolecular Ln···Ln distance belonging to 1-Pr (11.0573(5) Å).

Magnetometry

The static magnetisation and $\chi_{\rm M}T$ were investigated for the paramagnetic analogues of 1-Ln (Ln = Ce, Pr, Nd). Room temperature $\chi_{\rm M}T$ values are slightly low but still in good agreement with their free-ion Curie constants (C), being 0.72 cm³ K mol⁻¹ for **1-Ce** (Ce(III), ${}^{2}F_{5/2}$, $C = 0.80 \text{ cm}^{3} \text{ K mol}^{-1}$), 1.50 cm³ K mol⁻¹ for 1-Pr (Pr(III), ${}^{3}H_{4}$, $C = 1.60 \text{ cm}^{3} \text{ K mol}^{-1}$) and 1.55 cm³ K mol^{-1} for **1-Nd** (Nd(III), ${}^{4}\text{I}_{9/2}$, $C = 1.64 \text{ cm}^{3} \text{ K mol}^{-1}$) (Fig. 3). ¹⁷ Ab initio calculated $\chi_{M}T$ products are also in good agreement with the measured results. The $\chi_{\rm M}T$ products steadily decrease

Paper Dalton Transactions

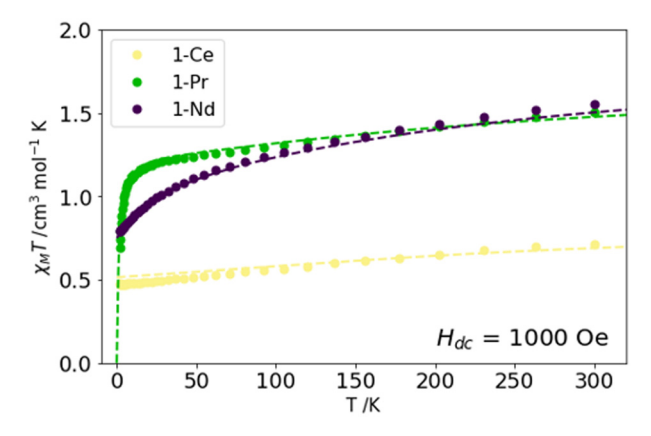


Fig. 3 Molar magnetic susceptibility (χ_M) temperature products of 1-Ln (Ln = Ce, cream; Ln = Pr, green; Ln = Nd, purple) between 2 and 300 K under an applied magnetic field (H_{dc}) of 1000 Oe. Experimental data are shown as solid circles and CASSCF-SO calculations as dashed lines.

before dropping more rapidly at low temperatures for all samples, though the rapid drop is most pronounced for **1-Pr**, likely indicating a marginal splitting in the pseudo-doublet ground state. The magnetization curves for **1-Ce**, **1-Pr** and **1-Nd** all show their desired saturation (Fig. S9 \dagger) at low temperature (T = 2, 4, 6 K) and are again in agreement with calculations.

To examine the effects of the Tp^{2-Fu} pseudo-icosahedral ligand field on SIM behaviour, alternating current (ac) magnetic susceptibility studies were performed on **1-Ce**, **1-Pr** and **1-Nd**. Firstly, **1-Pr** does not present any pronounced out-of-phase magnetic susceptibility (χ ") signals regardless of applied fields (T = 2-20 K, Fig. S12 and S13†), implying **1-Pr** is not a SIM. Based on the behaviour of **1-Ce** and **1-Nd**, *vide infra*, the use of the non-Kramers ion praseodymium(III) and weakly perturbing icosahedral crystal field (which is observed in **2-Ln**)¹³ has been attributed to the poor behaviour of **1-Pr**.

The zero-field behaviour of **1-Nd** shows frequency dependence in χ'' only below 5 K; however, no peaks are present (Fig. S15†). Applied field ($H_{\rm dc}=2000$ Oe) studies on **1-Nd** reveal peaks in χ'' between 2 and 4 K (Fig. 4 left and Fig. S18†), which were fitted to the generalised Debye equation (eqn (S1)†) to extract the magnetic relaxation times (τ) that were further modelled using a magnetic relaxation rate equation

(eqn (S2)†). Plotting the natural logarithm of the magnetic relaxation times against inverse temperature (T^{-1}) produces a non-linear regime, likely indicating Raman relaxation (Fig. S19†). Thus, these were fitted employing the Raman relaxation rate equation, $\tau^{-1} = CT^n$, yielding the values C = 0.028(7) s⁻¹ K⁻ⁿ and n = 10.3(2).

The Raman exponent of 10.3(2) is unusually large for a Kramers ion, where reduced exponents are typically sought to improve SIM behaviour. When attempting to fit the magnetic relaxation rates for 1-Nd to an Orbach style equation, an energy barrier of $U_{\rm eff}=19.9(5)~{\rm cm}^{-1}~(\tau_0=3.0(9)\times 10^{-8}~{\rm s})$ is extracted. Despite it being similar to those of other reported neodymium(III) based SIMs, we note that the data points do not fit as well as for the purely Raman relaxation mechanism (Fig. S19†). We attribute the dominant Raman relaxation mechanism to the large ligand scaffold likely having a high density of low energy vibrational modes.

Surprisingly, the zero-field magnetic susceptibility for 1-Ce showed frequency and temperature dependence up to 15 K when using frequencies up to 10 000 Hz and the sensitivity of cerium(III) based zero-field SIMs is highlighted by the high adiabatic susceptibility, indicating that a large percentage of the sample does not show slow relaxation under zero-field conditions. To date, only two other cerium(III) compounds have been reported as zero-field SIMs, [Ce(Cp^{ttt})₂Cl] (Cp^{ttt} = 1,2,4-tritert-butylcyclopentadineyl), though the authors only refer to the applied field data ($H_{dc} = 1000$ Oe), and [Ce{ZnI $(L)_{2}$ (MeOH)](BPh₄) (L = N,N,O,O-tetradentate Schiff base), with an effective anisotropic energy barrier of $U_{\text{eff}} = 14.7(4)$ cm⁻¹.^{20,21} The zero-field relaxation parameters for [Ce (Cpttt)2Cl] are included in their ESI and showed both Raman and quantum tunnelling of magnetisation (QTM) relaxation mechanisms, with applied field magnetic relaxation displaying solely Raman relaxation (Table 2).20 Upon reviewing the zerofield data for [Ce(Cpttt)2Cl], it seems the fitting to the generalised Debye equation at 2 K was not modelled appropriately, producing a non-existent QTM mechanism.

Zero-field ac magnetic susceptibilities for **1-Ce** were collected between 2 and 8 K (Fig. 4 and Fig. S16 \dagger). Fitting this data to the generalised Debye equation resulted in distribution parameters (α) below 0.02, indicating a narrow distribution of magnetic relaxation times (Table S2 \dagger). The χ'' at low tempera-

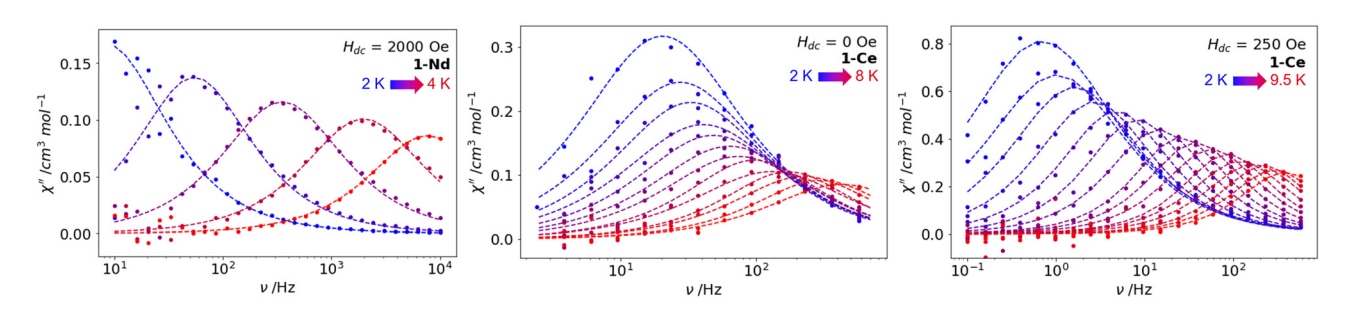


Fig. 4 Out-of-phase (χ'') magnetic susceptibility data for **1-Nd** under an applied field (H_{dc} = 2000 Oe; 2–4 K; left), **1-Ce** in zero-field (H_{dc} = 0 Oe, 2–8 K; middle) and **1-Ce** under an applied field (H_{dc} = 250 Oe; 2–9.5 K; right). Temperature gradients are from blue (low temp) to red (high temp), where dashed lines are fits to the generalised Debye equation (R^2 > 0.90).

Dalton Transactions Paper

Table 2 Relaxation parameters for zero and applied field cerium-based SIMs^{13,19–21}

		Orbach		Raman		om.
Complex	$H_{ m dc}/{ m Oe}$	τ_0/s	$U_{\rm eff}/{\rm cm}^{-1}$	$C/s^{-1} K^{-n}$	n	$ m QTM \ au_{QTM}/s$
1-Ce	0	$2.7(3) \times 10^{-6}$	30(5)	54(7)	1.2(1)	
	250	$1.2(2) \times 10^{-5}$	25.1(6)	0.9(1)	2.2(1)	_
2-Ce	1500	_ ` ´	_ ` `	6.9(6)	4.34(5)	_
[Ce(Cp ^{ttt}) ₂ Cl]	0^a	_	_	1.28×10^{-3}	8.28	1.74×10^{-2}
- (1 /- 1	1000	_	_	4.75×10^{-3}	6.48	_
$[Ce{ZnI(L)}_2(MeOH)](BPh_4)^b$	0	$1.6(3) \times 10^{-7}$	14.7(4)	_	_	$3.8(2) \times 10^{-4}$
[Ce(NO ₃) ₃ (1,10-diaza-18-crown-6)]	1000	$2.3(5) \times 10^{-8}$	31(1)	0.54(2)	5 ^c	

^a Zero-field behaviour may not be reported accurately (see in text). ^b The switch to a non-linear regime is identified as QTM though it is possible that this divergence is a consequence of Raman relaxation as at the time of publishing it was not widely adopted. ^c Value was fixed during fitting.

ture for 1-Ce bears a resemblance to the behaviour of 2-Tb;¹³ there is a limiting value for χ'' at high frequency below 5.5 K before temperature dependence emerges above the said temperature. For 2-Tb, this behaviour was indicative of the switching between Raman and Orbach relaxation. After plotting the relaxation times for 1-Ce, the same is true where above 5.5 K there is a switch from Raman to Orbach relaxation. The relaxation rate fitting for 1-Ce produces an effective energy barrier to magnetic relaxation of $U_{\rm eff} = 30(5)~{\rm cm}^{-1}$ and Raman parameters of C = 53(2) s⁻¹ K⁻ⁿ and n = 1.26(6) (Fig. 5). Notably, the zero-field ac susceptibility for 1-Ce does not present magnetic relaxation via a QTM mechanism, implying that the cerium centres are well isolated from each other (shortest intermolecular distance of Ce···Ce = 11.0781(6) Å), which differs from $[Ce(Cp^{ttt})_2Cl]$ (Ce···Ce = 8.0712(5) Å) where an applied field was reportedly needed to supress QTM.²⁰

Applied-field sweeps at 2 K (Fig. S11†) revealed the optimal applied field for magnetic relaxation in **1-Ce** to be $H_{\rm dc}=250$ Oe, with the applied field data bearing a resemblance to the zero-field susceptibility, though magnetic relaxation is slower at a given temperature (Fig. 4). Applied-field ac data for **1-Ce** were analysed analogously to the zero-field data, yielding

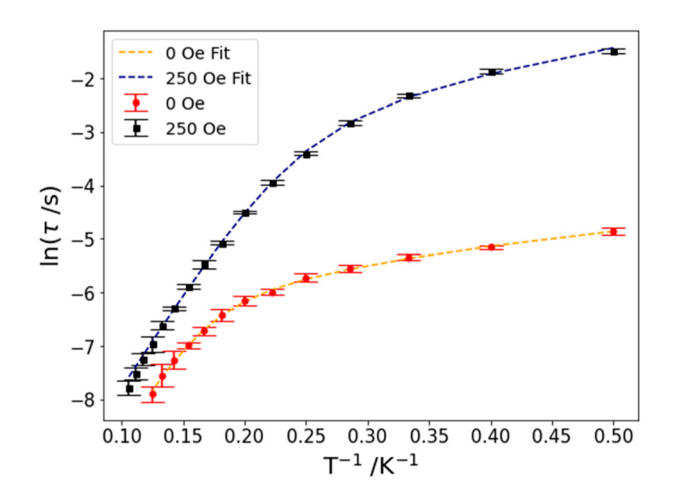


Fig. 5 Magnetic relaxation plots for 1-Ce under zero and applied magnetic fields. Both data sets have been modelled using Orbach and Raman fitting with parameters summarised in Table 2.

a similar energy barrier (Fig. 5 and Table 2). The same limiting phenomenon was observed in the applied field data for **1-Ce**; however, the switching temperature was lower at ca. 4 K. The energy barrier derived from the fitting for **1-Ce** in zero-field is, to our knowledge, the highest for a cerium-based SIM but is approximately equal to the record of 31(1) cm⁻¹ (within error), observed for [Ce(NO₃)₃(1,10-diaza-18-crown-6)] in an applied field (Table 2),²² and is a rare example where zero-field behaviour is observed, although we do acknowledge that a small residual field might be the cause of said zero-field behaviour.

Ab initio calculations

To gain insight into the magnetic properties of 1-Ln, complete-active space self-consistent field spin-orbit (CASSCF-SO) calculations were performed. The total splitting of the ground spin-orbit coupled term in 1-Ln is more pronounced than in 2-Ln, where the total splitting in 1-Ln is between 501 and 768 cm⁻¹ (cf. the largest splitting of 407 cm⁻¹ within the bis-Tp^{2-py} moiety in 2-Dy).¹³ To determine if the charge density, i.e. the electronic field created by the ligand environment, is different when comparing Tp^{2-py} to Tp^{2-Fu}, the LoProp charges were extracted from the CASSCF-SO calculations. The charges on the metal centres are slightly higher in the bis-Tp2-Fu systems, being 2.45 on average (cf. 2.40 in 2-Ln), 13 along with higher negative charges on the coordinating $N_{\rm pz}$ and $O_{\rm Fu}$ atoms of -0.36 and -0.35 (Table S8†), respectively. The resulting higher magnitude charges, when employing an electrostatic model, are responsible for the increased crystal field splitting, but due to the pseudo-sphere distribution of charge, the total splitting is still relatively low cf. other bis-axial ligand environments. 1-3,5-11 In all cases, the crystal fields in 1-Ln are defined along the g_z direction due to the presence of axial anisotropy created by the bis-Tp^{2-Fu} ligand environment. The highest magnitude m_I states for each ion in **1-Ln** become less oblate from cerium to neodymium which is reflected by the increasing deviation of the ground state quantisation axis from the B···B axis (Fig. S20-S22†), an increase in the degree of mixing in the ground states and a reduction in the g_z values from the Ising-limit.²³

Table 3 Calculated energies, g_z values for pseudo-doublets and wavefunction compositions for the non-Kramers ion containing **1-Pr**

Energy/cm ⁻¹	g_z	Wavefunction composition ^a
0	5.9644	$0.47 +4\rangle + 0.47 -4\rangle$
2.70		$0.48 +4\rangle + 0.48 -4\rangle$
48.9	_	$0.44 +3\rangle + 0.44 -3\rangle$
142	2.3772	$0.47 +2\rangle + 0.47 -2\rangle$
151		$0.33 -2\rangle + 0.33 -2\rangle + 0.12 +1\rangle + 0.12 -1\rangle$
234	_	$0.44 +3\rangle + 0.44 -3\rangle$
556	1.2040	$0.41 +1\rangle + 0.41 -1\rangle + 0.12 0\rangle$
563		$0.35 +1\rangle + 0.35 -1\rangle + 0.12 +2\rangle + 0.12 -2\rangle$
768	_	0.77 0>

^a Contributions under 10% are not shown.

The ground state of the non-Kramers praseodymium(III) ion in **1-Pr** reflects that of a pseudo-doublet with states 2.70 cm⁻¹ apart (Table 3). The relatively large energy gap within this ground pseudo-doublet is likely the reason for the fast magnetic relaxation in **1-Pr**. The wavefunction decomposition reveals that the $3^{\text{rd}}/4^{\text{th}}$ and $6^{\text{th}}/7^{\text{th}}$ excited states are pseudo-doublets with slightly larger energy separation (Table 3). In a perfectly axial crystal field, there would be no wavefunction mixing for non-Kramers ions, and all energies would be doublet states with a singlet state of $m_J = 0$. This type of electronic structure is approximately established when stronger crystal fields are used and are not as susceptible to deviations from axial crystal fields.

As stated, the Kramers ions (neodymium(III)) and cerium(III)) prefer axial anisotropy for their ground states, although the m_J = $\pm 9/2$ state for neodymium(III) is more isotropic than cerium (III) (with respect to its electrostatic potentials). ^{12,23} For **1-Nd**, we find that the ground state wavefunction composition is 67% $m_J = \pm 7/2$ while the first excited state possesses a higher composition of the $m_J = \pm 9/2$ state at 51%. All states in the ground *J*-manifold for **1-Nd** are heavily mixed and the first excited state sits 20.5 cm⁻¹ above the ground state. This energy gap is comparable to the Orbach relaxation parameter derived from the magnetometry data, suggesting that an Orbach mechanism is probable for **1-Nd**.

The electronic structure for **1-Ce** is a simpler example as there are only 3 doublets that define the *J*-manifold. The ground state of **1-Ce** is highly axial $(g_x = 0.13, g_y = 0.23, g_z = 4.05)$ and well defined by $m_J = \pm 5/2$, with the projection of this state deviating from the B···B axis by 0.9° (Fig. S20†). The ground state is highly stabilised with the first and second excited states in **1-Ce** sitting 532 and 572 cm⁻¹ above the ground state. The first and second excited states are predominately defined by $m_J = \pm 1/2$ and $\pm 3/2$, respectively (Table 4), and are not sequentially ordered; thus magnetic relaxation could occur *via* the first excited state. However, like most cerium-based SIMs, the experimental energy barrier to magnetic relaxation is less than 50 cm⁻¹ even though the first excited state sits an order of magnitude higher than this.

Previous exploration by Rajaraman and co-workers looked into a similar cerium(III) problem and attempted RAS-probing calculations to explore if 4d orbitals contributed to the crystal field splitting states, to no avail.²⁴ We explored an alternative

Table 4 Calculated energies, g_z values and angle of the projection of the state compared to the ground state, and wavefunction contributions for the Kramers ion containing **1-Ce** and **1-Nd**

	Energy/cm ⁻¹	g_z	Angle/°	Wavefunction compositions ^a
1-Ce	0	4.05	_	0.99 ±5/2>
	532	2.84	80.99	$0.81 \pm 1/2\rangle + 0.15 \pm 3/2\rangle$
	572	2.68	43.32	$0.84 \pm 3/2\rangle + 0.13 \pm 1/2\rangle$
1-Nd	0	4.88	_	$0.67 \pm 7/2\rangle + 0.16 \pm 9/2\rangle$
				$+0.13 \pm 5/2\rangle$
	20.5	5.15	16.85	$0.51 \pm 9/2\rangle$
				$+0.22 \pm 3/2\rangle + 0.16 \pm 7/2\rangle$
	150	1.82	86.83	$0.38 \pm 3/2\rangle + 0.28 \pm 5/2\rangle$
				$+0.12 \pm1/2\rangle$
	397	2.33	82.54	$0.39 \pm 5/2\rangle + 0.27 \pm 1/2\rangle$
				$+0.11 \pm 3/2\rangle$
	501	3.8146	11.43	$0.42 \pm 3/2\rangle + 0.32 \pm 9/2\rangle +$
				$0.12 \pm 1/2\rangle + 0.12 \pm 5/2\rangle$

^a Contributions under 10% are not shown.

avenue, performing calculations including the 5d orbitals in the RAS3 space. However, similar to the prior computational studies, we found minimal variations in the calculated results (Table S9†). Computational variations are ongoing, focusing on the double shell effect (5f orbitals) as well as the impact of simultaneous inclusion of 4d and 5d orbitals in RAS probing methods. However, to date, an explanation for the low experimentally observable cerium(III) energy barriers remains an unexplained phenomenon.

Conclusions

The introduction of a new pseudo-icosahedral crystal field to generate single-ion axial anisotropy has been achieved with the use of the hexadentate Tp^{2-Fu} ligands. The synthesis of **1-Ln** for the early lanthanides yields SIM behaviour for Kramers ions and, for the case of cerium(III) where the ground state is oblate, provides a rare case of a zero-field single-ion magnet. Unlike Tp^{2-py}, the use of a heteronuclear scorpionate ligand that supports an equatorial belt of oxygen donors produces a greater overall perturbation of the ground J-manifold due to the higher partial charges on the donor atoms. The pseudo-I_c crystal field in **1-Ce** stabilises a ground state that is predominantly $m_J = \pm 5/2$ and sits over 500 cm⁻¹ below the first excited state, which is a key property for cerium(III)-based SIMs. Magnetic characterisation by ac susceptibility measurements produces an energy barrier to magnetic relaxation of 30(5) cm⁻¹, which is significantly smaller than the calculated energy of the first excited state. Additional CASSCF calculations that incorporate the 5d orbitals into the active space did not shed light on this discrepancy, which remains an unanswered question in the literature.

Author contributions

Jarrod R. Thomas: synthetic work, single-crystal XRD collection and analysis, collection and analysis of magnetic data, and collection of spectroscopic data; Marcus J. Giansiracusa: *ab initio* calculations and collection and analysis of magnetic data; Jonathan T. Mifsud: synthetic work; Richard A. Mole: collection of magnetometry data; Scott A. Sulway: directed the research.

Data availability

Computational data is available free of charge at https://doi.org/10.26188/27266358. Crystallographic data for 1-Ln have been deposited at the CCDC under codes 2395485–2395488. The data supporting this article are included as part of the ESI.†

Conflicts of interest

There are no conflicts to declare.

Acknowledgements

This research was supported by The University of Melbourne's Research Computing Services and the Petascale Campus Initiative. This work was performed in part at the Trace Analysis for Chemical, Earth and Environmental Sciences (TrACEES) Platform University Melbourne. M. J. G. would like to thank the University of Melbourne for funding. S. A. S. and J. R. T. would like to thank the University of New South Wales for their funding. The authors would like to thank ANSTO for facilitating access to use the PPMS via P17507 and acknowledge the Australian Research Council for their equipment grant (LE210100009). The authors would also like to acknowledge the Mark Wainwright Analytic Centre (MWAC) for aid in and use of their instrumentation for the collection of single-crystal X-ray diffraction data, NMR data at the NMR facility, and microanalysis through the XRF laboratory.

References

- 1 F. Guo, B. M. Day, Y. Chen, M. Tong, A. Manskkamaki and R. Layfield, Magnetic hysteresis up to 80 Kelvin in a dysprosium metallocene single-molecule magnet, *Science*, 2018, **362**, 1400–1403.
- 2 C. A. P. Goodwin, F. Ortu, D. Reta, N. F. Chilton and D. P. Mills, Molecular magnetic hysteresis at 60 Kelvin in dysprosocienium, *Nature*, 2017, 548, 439–442.
- 3 K. R. McClain, C. A. Gould, K. Chakarawet, S. J. Teat, T. J. Groshens, J. R. Long and B. G. Harvey, High-temperature magnetic blocking and magneto-structural correlations in a series of dysprosium(III) metallocenium singlemolecule magnets, *Chem. Sci.*, 2018, 9, 8492–8503.
- 4 J. R. Thomas, M. G. Giansiracusa and S. A. Sulway, Approaching the 1000 K energy barrier in high coordinate

- lanthanide single-ion magnets: Increasing U_{eff} in the [Dy $(\mathrm{Tp}^{2-\mathrm{py}})\mathrm{F}]^+$ moiety with tetrahydrofuran, *Dalton Trans.*, 2024, 53, 9252–9256.
- 5 J. C. Vanjak, B. O. Wilkins, V. Vieru, N. S. Bhuvanesh, J. H. Reibenspies, C. D. Martin, L. F. Chibotaru and M. Nippe, A high-performance single-molecule magnet utilizing dianionic aminoborolide ligands, *J. Am. Chem. Soc.*, 2022, 144, 17743–17747.
- 6 A. H. Vincent, Y. L. Whyatt, N. F. Chilton and J. R. Long, Strong axiality in a dysprosium(III) bis(borolide) complex leads to magnetic blocking at 65 K, *J. Am. Chem. Soc.*, 2023, 145, 1572–1579.
- 7 C. A. Gould, K. R. McClain, J. M. Yu, T. J. Groshens, F. Furche, B. G. Harvey and J. R. Long, Synthesis and magnetism of neutral, linear metallocene complexes of terbium(II) and dysprosium(II), J. Am. Chem. Soc., 2019, 141, 12967–12973.
- 8 J. Emerson-King, G. K. Gransbury, G. F. S. Whitehead, I. J. Vitorica-Yrezabal, M. Rouzières, R. Clérac, N. F. Chilton and D. P. Mills, Isolation of a bent dysprosium bis(amide) single-molecule magnet, *J. Am. Chem. Soc.*, 2024, 146, 3331–3342.
- 9 H. Kwon, K. R. McClain, J. G. C. Kragskow, J. K. Staab, M. Ozerov, K. R. Meihaus, B. G. Harvey, E. S. Choi, N. F. Chilton and J. R. Long, Coercive fields exceeding 30 T in the mixed-valence single-molecule magnet (Cp^{iPr5})₂Ho₂I₃, J. Am. Chem. Soc., 2024, 146, 18714–18721.
- 10 (a) S. C. Corner, G. K. Gransbury, I. J. Vitorica-Yrezabal, G. F. S. Whitehead, N. F. Chilton and D. P. Mills, Halobenzene adducts of a dysprosocenium single-molecule magnet, *Inorg. Chem.*, 2024, 63, 9552–9561; (b) S. C. Corner, G. K. Gransbury, I. J. Vitorica-Yrezabal, G. F. S. Whitehead, N. F. Chilton and D. P. Mills, Synthesis and magnetic properties of bis-halobenzene decamethyldysprosocenium cations, *Inorg. Chem.*, 2024, 63, 9562–9571.
- 11 P.-B. Jin, Q.-C. Luo, G. K. Gransbury, I. J. Vitorica-Yrezabal, T. Hajdu, I. Strashnov, E. J. L. McInnes, R. E. P. Winpenny, N. F. Chilton, D. P. Mills and Y.-Z. Zheng, Thermally stable terbium(II) and dysprosium(II) bis-amindinate complexes, *J. Am. Chem. Soc.*, 2023, 145, 27993–28009.
- 12 (a) J. D. Rinehart and J. R. Long, Exploiting single-ion anisotropy in the design of f-element single-molecule magnets, *Chem. Sci.*, 2011, 2, 2078–2085; (b) A. Borah and R. Murugavel, Magnetic relaxation in single-ion magnets formed by less-studied lanthanide ions Ce(III), Nd(III), Gd (III), Ho(III), Tm(II/III) and Yb(III), *Coord. Chem. Rev.*, 2022, 453, 214288–214302.
- 13 J. R. Thomas, M. J. Giansiracusa, R. A. Mole and S. A. Sulway, Increasing the symmetry around lanthanide ions: the effect on single-ion magnet behavior and electronic structure, *Cryst. Growth Des.*, 2024, 24, 573–583.
- 14 J. R. Thomas and S. A. Sulway, Borotropic shifting of the hydrotris[3-(2-furyl)pyrazol-1-yl]borate ligand in high-coordinate lanthanide complexes, *Acta Crystallogr.*, *Sect. C: Cryst. Struct. Commun.*, 2024, C80, 153–158.
- P. L. Jones, A. J. Amoroso, J. C. Jeffery, J. A. McCleverty,
 E. Psillakis, L. H. Rees and M. D. Ward, Lanthanide

Paper

Complexes of the Hexadentate N-Donor Podand Tris[3-(2-pyridyl)pyrazolyl]hydroborate: Solid-State and Solution Properties, *Inorg. Chem.*, 1997, **36**, 10–18.

- 16 A. J. Amoroso, J. C. Jeffery, P. L. Jones, J. A. McCleverty, L. Rees, A. L. Rheingold, Y. Sun, J. Takats, S. Trofimenko, M. D. Ward and G. P. A. Yap, Complexes of the podand ligand tris[3-(2-pyridyl)-pyrazol-1-yl)borate with lanthanoids and actinoids: rare examples of icosahedral N₁₂ coordination, J. Chem. Soc., Chem. Commun., 1995, 1881–1882.
- 17 *The Rare Earth Elements: Fundamentals and Applications*, ed. D. A. Atwood, John Wiley & Sons Ltd, 2005.
- 18 (a) E. Garlatti, A. Chiesa, P. Bonfà, E. Macaluso, I. J. Onuorah, V. S. Parmar, Y.-S. Ding, Y.-Z. Zheng, M. J. Giansiracusa, D. Reta, E. Pavarini, T. Guidi, D. P. Mills, N. F. Chilton, R. E. P. Winpenny, P. Santini and S. Carretta, A cost-effective semi-ab initio approach to model relaxation in rare-earth single-molecule magnets, *J. Phys. Chem. Lett.*, 2021, 12, 8826–8832; (b) A. Borah, S. Dey, S. K. Gupta, G. Rajaraman and R. Murugavel, Field-indiced SIM behaviour in early lanthanide(III) organophosphates containing 18-crown-6, *Dalton Trans.*, 2023, 52, 8943–8955.
- 19 (a) S. K. Gupta, T. Rajeshkumar, G. Rajaraman and R. Murugavel, An unprecedented zero field neodymium(III) single-ion magnet based on a phosphonic diamide, *Chem. Commun.*, 2016, 52, 7168–7171; (b) J. D. Rinehart and J. R. Long, Slow magnetic relaxation in homoleptic trispyrazolylborate complexes of neodymium(III) and uranium(III), *Dalton Trans.*, 2012, 41, 13572–13574; (c) J. J. Le Roy, S. I. Gorelsky, I. Korobkov and M. Murugesu, Slow magnetic relaxation in uranium(III) and neodymium(III)

- cyclooctatetraenyl complexes, *Organometallics*, 2015, 34, 1415–1418; (*d*) A. Arauzo, A. Lazarescu, S. Shova, E. Bartolomé, R. Cases, J. Luzón, J. Bartolomé and C. Turta, Structural and magnetic properties of some lanthanide (Ln = Eu(III), Gd(III) and Nd(III)) cyanoacetate polymers: Field-induced slow magnetic relaxation in the Gd and Nd substitutions, *Dalton Trans.*, 2014, 43, 12342–12356; (*e*) A. K. Jassal, N. Aliaga-Alcalde, M. Corbella, D. Aravena, E. Ruiz and G. Hundal, Neodymium 1D systems: Targeting new sources for field-induced slow magnetization relaxation, *Dalton Trans.*, 2015, 44, 15774–15778.
- 20 J. Liu, D. Reta, J. A. Cleghorn, Y. X. Yeoh, F. Ortu, C. A. P. Goodwin, N. F. Chilton and D. P. Mills, Light lanthanide metallocenium cations exhibiting weak equatorial anion interactions, *Chem. – Eur. J.*, 2019, 7749–7758.
- 21 S. Hino, M. Maeda, K. Yamashita, Y. Kataoka, M. Nakano, T. Yamamura, H. Nojiri, M. Kofu, O. Yamamura and T. Kajiwara, Linear trinuclear Zn(II)–Ce(III)–Zn(II) complex which behaves as a single-molecule magnet, *Dalton Trans.*, 2013, 42, 2683–2686.
- 22 H. Wada, S. Ooka, T. Yamamura and T. Kajiwara, Light lanthanide complexes with crown ether and its aza derivative which show slow magnetic relaxation behaviors, *Inorg. Chem.*, 2017, **56**, 147–155.
- 23 J.-L. Liu, Y.-C. Chen and M.-L. Tong, Symmetry strategies for high performance lanthanide-based single-molecule magnets, *Chem. Soc. Rev.*, 2018, 47, 2431–2453.
- 24 S. K. Singh, T. Gupta, L. Ungur and G. Rajaraman, Magnetic relaxation in single-electron single-ion cerium (III) magnets: Insights from ab initio calculations, *Chem. – Eur. J.*, 2015, 21, 13812–13819.